Chapter 3

Rate-effects and Shock Formation in the Impacted VACNT Foams[2]

In this chapter, we investigate the rate-effects on the dynamic response of VACNT foams excited by impacts at controlled velocities. They exhibit a complex rate-dependent loading-unloading response at low impact velocities and they support shock formation beyond a critical velocity. The measured critical velocities are ~10 times lower than in other foams of similar densities—a desirable characteristic in impact protective applications. *In-situ* high-speed microscopy reveals strain localization and progressive buckling at low velocities and a crush-front propagation during shock compression. We correlate these responses to quantitative measurements of the density gradient and fiber morphology, obtained with spatially resolved X-ray scattering and attenuation. We also show that the dynamic properties can be significantly tailored by affecting the nanostructure (number of walls, diameter and alignment of CNTs) of the VACNT foams that results in various controlled bulk densities between 0.1-0.3 g cm^{-3}.

3.1 Introduction

Carbon nanotube (CNT) arrays can be fabricated to different scales: from microscopic, regular patterns of individual tubes for electronic and sound applications [93,139,140], to bulk and entangled macrostructures, for mechanical and textile applications [95,96]. For example, long fibers and yarns have been produced for bulletproof tough textiles and conductive electronic textiles [95,96]. Sheets of CNTs have been fabricated for transparent highly elastomeric electrodes [32] and underwater thermoacoustic projectors

[2] This chapter is adapted from the paper authored by R. Thevamaran, E. R. Meshot and C. Daraio [166]. RT and CD designed the study. RT synthesized samples, performed mechanical characterization and analyzed the data. ERM designed and conducted the synchrotron x-ray scattering experiments. RT wrote the manuscript with the support of CD and ERM. All authors contributed to the interpretation of the results and writing of the manuscript.

[93]. Thin film bucky papers made of randomly oriented individual carbon nanotubes have also been studied for energy storage and chemical catalysis [141,142]. In bulk, vertically aligned carbon nanotube (VACNT) arrays [37,140,143] and non-aligned inter-connected sponge like structures [55] have been investigated for energy dissipative cushioning and packaging, super-capacitor, catalytic electrodes, super hydrophobic surfaces and scaffolds for tissue engineering. Freestanding VACNT arrays exhibit an intriguing mechanical response that, for example, makes them the most efficient low-density, energy absorbing material known [37,63,72]. These properties arise from their intrinsic complex deformation behavior, which opens up fundamental areas of investigation in mechanics, and serves as a controlled model to understand the response of hierarchical materials with a fibrous morphology.

Macroscale VACNT foams have constituents at different length scales, forming a hierarchical structure: entangled individual multi-walled carbon nanotubes (MWCNTs) at the nanoscale, a seemingly disordered forest at the microscale, and vertically aligned bundles at the mesoscale. The properties and morphologies of the constituent structures are highly dependent on the synthesis conditions [40] and they play an important role in determining the mechanical response of the bulk foams. Subjected to quasistatic compressive loading, freestanding VACNT foams exhibit super-compressibility and have the ability to recover from large strains of up to 80% upon unloading [37,144]. Their deformation response is highly localized and in compression these foams support the formation of sequential buckles, originating from anisotropic, graded functional properties. They also show high fatigue resistance, surviving tests of up to a million compressive cycles at moderate strains [38]. The fundamental characteristics of nucleation and propagation of sequential periodic buckling, observed first at the macro-scale [37], was confirmed in micro-pillars using *in-situ* indentation experiments inside a scanning electron microscope (SEM) [123,145].

Studies of rate effects on the mechanical response of bulk CNT foams have focused on the quasistatic regime or on the linear dynamic regime. Uniaxial compression cycles performed at up to 80% strain in the quasistatic regime (10^{-4}-10^{-1} s^{-1}) have shown a rate-independent mechanical response [62]. In contrast, faster, but still quasi-static, strain

rates (up to 0.04 s^{-1} [63] and up to 1 s^{-1} [64]) suggested rate effects on recovery [63] and unloading modulus [63,64]. In both reports the recovery and elastic unloading modulus were shown to increase with increasing deformation rates. In the linear dynamic regime, uniaxial nano-dynamic mechanical analysis (nano-DMA) at small amplitudes (3-50 nm; 0.7% strain) showed no dependence of the CNT foam's response on the driving frequency [65]. However, they reported the dependence of the storage and loss moduli on the driving amplitude and the variation of the foam's microstructure. Large amplitude DMA performed in torsion-mode (shear) also exhibited temperature and frequency invariant viscoelasticity between 0.1-100 Hz and -196-1000 ^{0}C [66]. Coarse-grained molecular dynamics simulations and triboelastic constitutive models supported these experimental observations [67]. It should be noted that the fundamental deformation mechanisms in uniaxial compression involving bending, buckling and microstructural rearrangements [37,65] are significantly different from the zipping, unzipping and bundling observed in torsion-mode (shear) DMA [66,67].

Drop-ball tests performed on VACNT forests demonstrated their ability to mitigate impacts [68,69] at high-rate deformations. However, the deformation behavior and the fundamental dissipative mechanisms at high rates and for finite deformations are not thoroughly understood due to the difficulties in obtaining dynamic displacement measurements with micro-scale resolutions.

Here, we report a detailed experimental study on the response of CNT foams subjected to controlled, high-rate impacts, reaching up to 95% strain, using time-resolved dynamic displacement and force measurements. This study provides a thorough understanding of fundamental dynamic deformation mechanisms in the micro- and macro-scales and identifies different dynamic regimes—localized buckling and shock formation—supported by VACNT foams.

3.2 Experimental methods

The VACNT foams presented in this chapter were synthesized using a floating catalyst thermal chemical vapor deposition (tCVD) process as described in Section 2.1.1. The resultant VACNT foams had thicknesses in the order of a millimeter. Hydrogen

concentration in the carrier gas was varied between 30% and 5% to produce VACNT foams with tailored microstructures and different bulk densities, varying from 0.1-0.3 g cm^{-3}. These different microstructures were shown to present mechanical properties varying over a broad range in the quasistatic regime [42]. The synthesized specimens were extracted from the substrate using a custom-made core drill and prepared for dynamic testing.

We performed synchrotron X-ray scattering and mass attenuation measurements to nondestructively quantify the density and alignment within the VACNT foams, as described in Section 2.2. The dynamic characterization of the VACNT foams was performed on the dynamic testing platform described in the Section 2.4. Details of the dynamic testing apparatus and the data reduction methods can be found in Section 2.4. The calculations of all mechanical parameters discussed in this chapter are described in the following section (Section 3.3).

3.3 Definition of parameters

Stress: The nominal stress (engineering stress) experienced by the specimen during impact, calculated by,

$$\sigma = \frac{F}{A}, \tag{3.1}$$

where F is the impact force measured by the dynamic force sensor and A is the initial area of the VACNT foam specimen.

Strain: The nominal strain (engineering strain) on the specimen, calculated by,

$$\varepsilon = \frac{\delta}{H}, \tag{3.2}$$

where δ is the dynamic displacement measured using the moiré interferometer and H is the initial height of the specimen.

Strain-rate: The effective strain rate at the moment of impact, given by,

$$\dot{\varepsilon} = \frac{V_{impact}}{H}, \tag{3.3}$$

where V_{impact} is the initial rate of deformation and H is the initial height of the specimen.

Unloading modulus: The gradient of the unloading curve on the stress-strain diagram at the beginning of unloading. It was calculated by,

$$E_{unloading} = \frac{\sigma(\varepsilon_{max}) - \sigma(0.95\,\varepsilon_{max})}{(\varepsilon_{max} - 0.95\,\varepsilon_{max})}, \tag{3.4}$$

where ε_{max} is the maximum strain attained during impact and $\sigma(\varepsilon_{max})$ denotes the stress corresponding to the ε_{max}.

Recovery: Percentage recovery of the specimen during unloading calculated by,

$$Percentage\ Recovery = \frac{\varepsilon_{max} - \varepsilon_f}{\varepsilon_{max}} \times 100. \tag{3.5}$$

Energy Dissipated: The hysteretic energy dissipation given by the area included within the hysteretic loop on the dynamic stress-strain diagram (Figure 3.1(a)).

$$W_{dissipated} = \oint \sigma \, d\varepsilon. \tag{3.6}$$

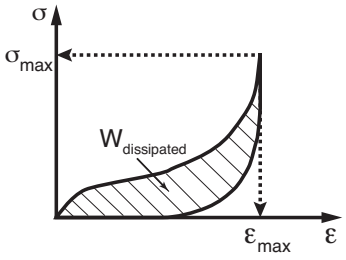

Figure 3.1 (a): Energy dissipated

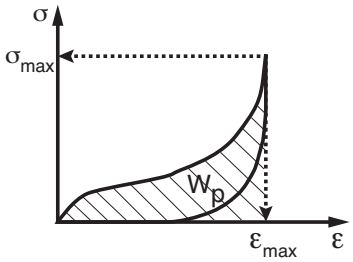

Figure 3.1 (b): Energy absorbed up to peak stress

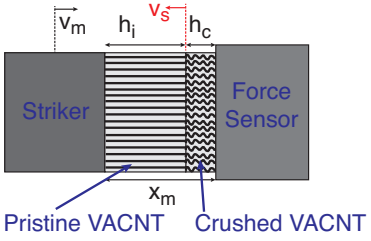

Figure 3.1 (c). Shock formation of VACNT foams

Dynamic cushion factor: The factor representing the damping characteristic of the VACNT foam. It was calculated by,

$$C_{dyn} = \frac{\sigma_p}{W_p}, \tag{3.7}$$

where σ_p is the peak stress and W_p is the energy absorbed up to the peak stress (Figure 3.1(b)) given by,

$$W_p = \int_0^{\sigma_p} \sigma \, d\varepsilon. \tag{3.8}$$

Definition of shock parameters (Figure 3.1(c)):

Striker velocity: The velocity at which the striker compresses the VACNT foam, defined by,

$$v_m = \frac{\Delta x_m}{\Delta t}, \tag{3.9}$$

where x_m is the current thickness of the VACNT foam. It is equivalent to the particle velocity of the intact VACNT foam in the case of a direct impact.

Crush front velocity: The velocity at which the sharp crush front progresses towards the striker, defined by,

$$v_c = \frac{\Delta h_c}{\Delta t}, \tag{3.10}$$

where h_c is the thickness of the crushed section of the VACNT foam.

Shock velocity: The velocity at which the shock wave propagates in the VACNT foam, defined by,

$$v_s = -\frac{\Delta h_i}{\Delta t}, \tag{3.11}$$

where h_i is the height of the pristine section of the VACNT foam that is not compressed by the shock.

3.4 Results and discussions

Our results of morphological characterization show a gradient in VACNT mass density for the synthesis conditions used in our study, with a monotonic decay towards the bottom (corresponding to the end of growth) (Figure 3.2 (a), (b)). This agrees with previous results for growth from substrate bound thin-film catalysts [146], but to our knowledge this is the first direct confirmation of density decay in floating catalyst growth of VACNTs.

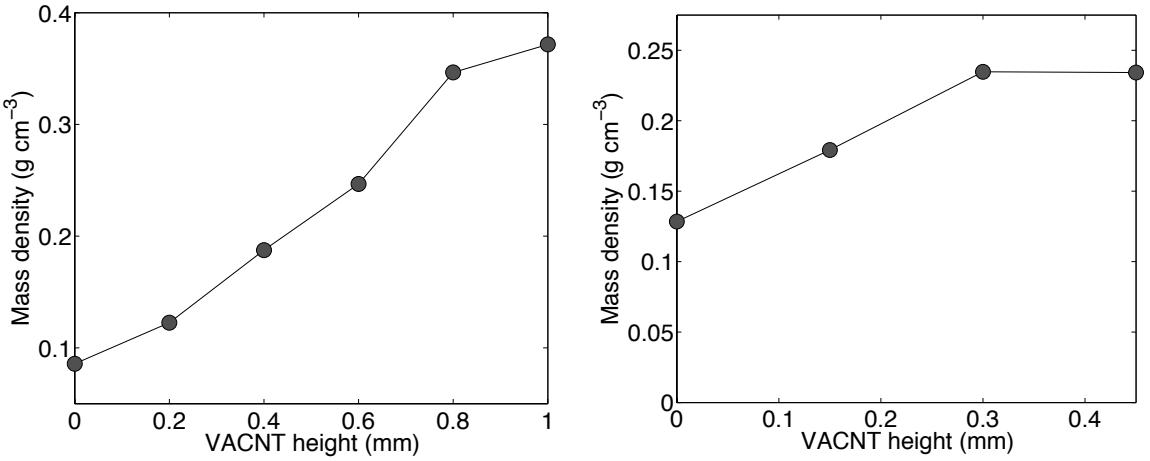

Figure 3.2. Characteristic intrinsic density variation along the height of the VACNT foam from the substrate: **(a)** for the sample that was synthesized using 5% H_2 concentration (measured mean density 0.23 g cm^{-3}), **(b)** the sample was synthesized using 15% H_2 concentration (measured mean density 0.19 g cm^{-3}). Zero is where the bottom of the beam meets the silicon substrate.

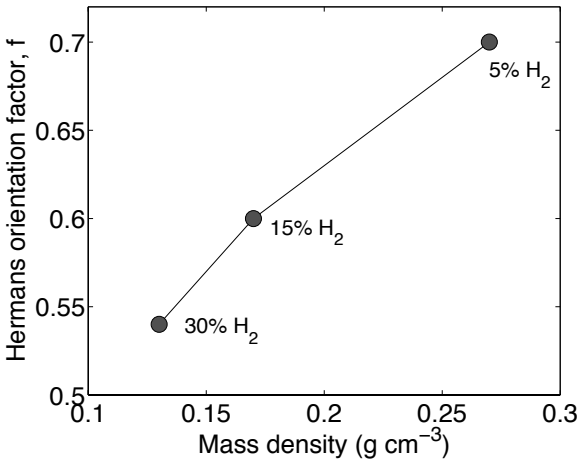

Figure 3.3. Direct correlation of alignment (*f*) with the mass density of VACNTs synthesized under the H_2 conditions in this study (5%, 15%, 30% concentration). Results from previous studies would suggest that this is a sublinear correlation, with *f* rapidly dropping to zero once a lower threshold of CNT density is reached [103].

Our CNTs are highly aligned with $f = 0.6$ on average, and we determined that alignment is directly correlated with density (Figure 3.3), which has a strong influence on the mechanical performance. The following results and discussion draw important quantitative relationships between the structural characteristics of the VACNT foams and their advanced mechanical properties.

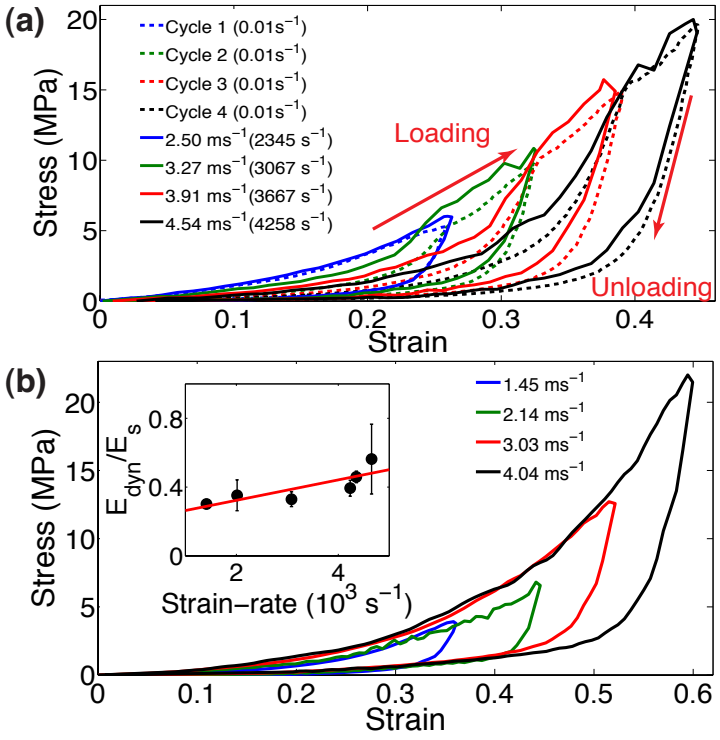

Figure 3.4. (a) Dynamic response of a VACNT foam subjected to several impacts at increasing controlled velocities (solid lines) compared to a similar VACNT foam subjected to quasistatic compressive cyclic loading (dashed lines). **(b)** Dynamic response of different pristine VACNT foams of similar densities, at increasing impact velocities. The inset shows the dynamic unloading modulus normalized by the quasistatic unloading modulus at given maximum strains reached during impact.

The effects of increasing loading rates on a VACNT foam are reported in Figure 3.4. We show a hysteretic response and the presence of preconditioning effects, similar to what was reported in the quasistatic regime [37,62]. The presence of hysteresis accounts for the dynamic energy dissipated on impact. The preconditioning effects are evident when the same specimen is impacted with increasing loading rates. During the first impact, the sample follows a large hysteretic path, characteristic of a pristine (as-grown) sample. As the sample is impacted again with a higher impact velocity, the loading path follows initially a preconditioned response, and then changes to that of the pristine specimen, when the strain exceeds the maximum strain reached in the prior impact (Figure 3.4 (a)). This behavior confirms the strain localization found in quasistatic tests [62]. In addition,

it demonstrates that the samples' loading responses are rate-independent, over a broad range of impact velocities from 1-6 m s^{-1} (nominal strain rates: 1000-6,000 s^{-1}). This rate-independent loading response is further verified by comparing the quasistatic compression cycles performed at 0.01 s^{-1} strain rate to the dynamic stress-strain cycles (Figure 3.4 (a)). To verify that the rate-independent loading response is not a function of a sample's loading history, we tested several pristine specimens at different impact velocities. A corresponding set of characteristic stress-strain curves is shown on Figure 3.4 (b).

The unloading response shows the presence of rate effects. This is verified by plotting the dynamic unloading modulus (E_{dyn}), normalized by the quasistatic unloading modulus (E_s), at maximum strain, against the nominal strain rate measured at the moment of impact (inset of Figure 3.4 (b)). This normalized unloading modulus increases with the strain rate, suggesting the presence of rate-effects during the recovery phase of the dynamic deformation.

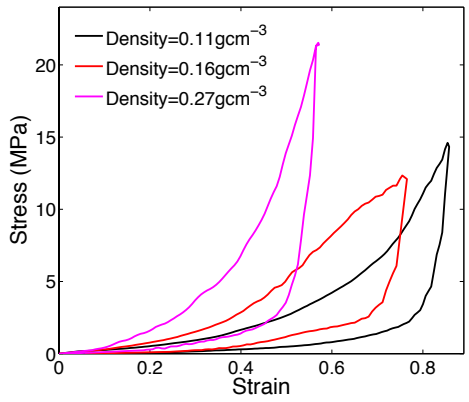

Figure 3.5. Characteristic dynamic stress-strain response of VACNT foams of different densities, subjected to an impact at a velocity of 3.78±0.18 m s^{-1}. As the VACNT foam's density decreases the response becomes increasingly compliant.

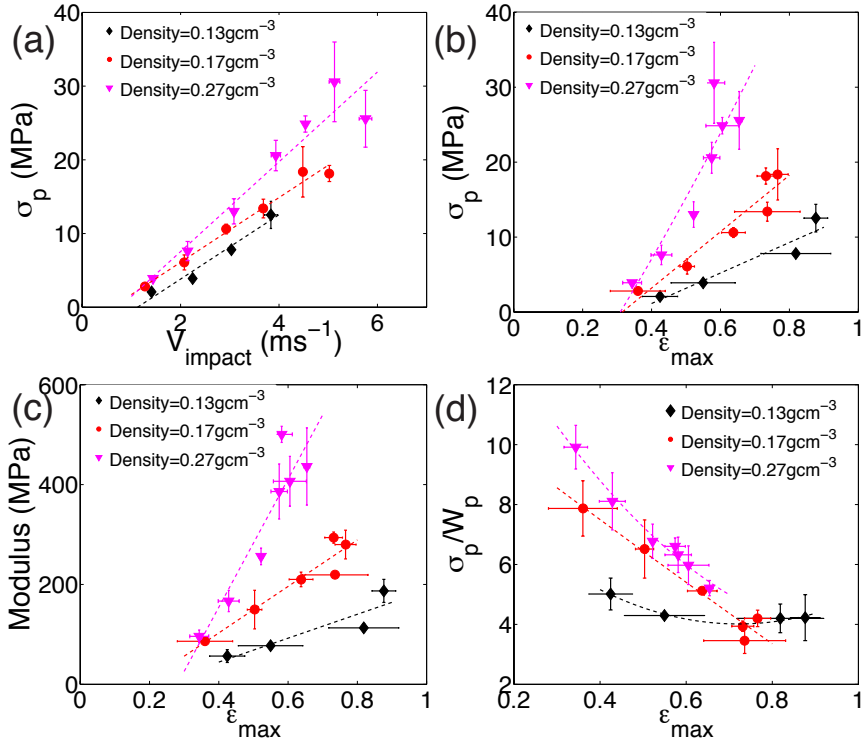

Figure 3.6. Dynamic response of VACNT foams with average bulk densities of 0.13±0.02, 0.17±0.02 and 0.27±0.02 g cm-3 (the horizontal and vertical error bars represent the standard deviation of the three samples tested in each case). **(a)** Variation of peak stress with the striker impact velocity; **(b)** variation of peak stress with the maximum strain reached during impact; **(c)** variation of the unloading modulus with the maximum strain reached during impact; **(d)** variation of the dynamic cushion factor—peak stress divided by energy absorbed up to peak stress—with the maximum strain reached during impact.

To explore the effects of a foam's microstructure on the bulk dynamic response, we performed similar experiments on VACNT foams with varying bulk densities (0.1-0.3 g cm^{-3}). A summary of the results can be found in Figures 3.5, 3.6 and 3.7. The peak stress increases with impact velocity (Figure 3.6 (a)) and maximum strain (Figure 3.6 (b)). It should be noted that the increase in the peak stress with impact velocity is not due to rate-effects, yet it is a natural consequence of the gradient in stiffness along the height of the foam as well as the densification that occurs during loading. Similar to peak stress, the unloading modulus also increases with the increasing maximum strain reached (Figure

3.6 (c)). The relation of the unloading modulus and the energy dissipation with increasing impact velocities is shown in Figures 3.7 (a) and (b). For a given impact velocity, VACNT foams with higher bulk densities exhibit stiffer responses characterized by higher peak stresses and unloading moduli.

We use the dynamic cushion factor, given by the peak stress divided by the energy absorbed up to the peak stress (σ_p/W_p), to characterize the damping efficiency of the VACNT foams. In general, a low cushion factor is beneficial for impact mitigation and energy dissipative applications. Both the increase in the energy absorption and the decrease in the peak stress contribute to reducing the cushion factor. To characterize the quasistatic response of conventional foam materials, the static cushion factor is plotted against the plateau stress [147]. This was also reported for the quasistatic response of disordered carbon nanotubes [56]. In dynamics, we plot (Figure 3.6 (d)) the cushion factor against the maximum strain reached to combine all the critical parameters of the impact response: the peak stress, maximum strain and the energy absorption. A conventional plot of the dynamic cushion factor with peak stress is given on Figure 3.7 (c).

VACNT foams with lower densities perform well in mitigating impact force and absorbing energy for a given maximum strain, at low velocity impacts (< 3 m s^{-1}; striker mass = 7.1 g), (Figure 3.6 (d)). When subjected to high velocity impacts, however, they rapidly reach the densification strain, posing a performance limit. VACNT foams with higher densities exhibit higher moduli and deform less and are capable of absorbing high velocity impacts. In the quasistatic regime, the energy dissipated by these VACNT foams was found to be more than 200 times higher than the energy dissipated by commercial foams of similar densities [72].

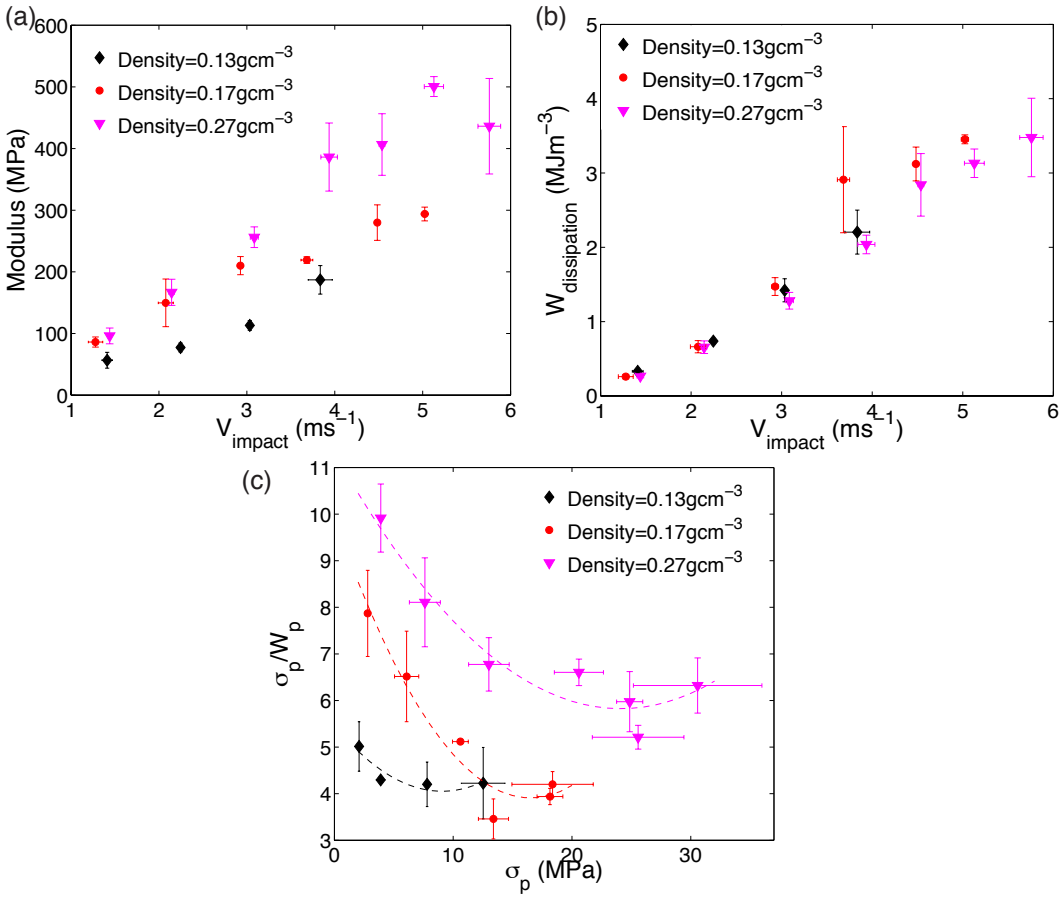

Figure 3.7 (a) Variation of unloading modulus with impact velocity. **(b)** Variation of hysteretic energy dissipation with impact velocity. **(c)** Variation of dynamic cushion factor with peak stress.

To compare the performance of the VACNT foams with that of other materials in the literature [59,148–151], we plot the elastic modulus as a function of the bulk density. For these plots, the unloading modulus of the VACNT foams was chosen over the loading modulus as the characteristic stiffness, since it represents the elastic recoiling of the VACNT foams after the impact (Figure 3.8). For the CNT foams, we show a range of dynamic unloading moduli arising from different maximum deformations reached at different impact velocities. For simplicity, they are grouped into three different ranges of maximum strains: 0.35-0.49 (with avg. 0.40), 0.50-0.69 (with avg. 0.60) and 0.70-0.88 (with avg. 0.75). The results follow a linear correlation in the double-logarithmic plot, implying a power-law relationship between the modulus and the density similar to the

one found in conventional foam materials [147]. VACNT foams always present the highest elastic moduli at a given bulk density when compared to other foam materials.

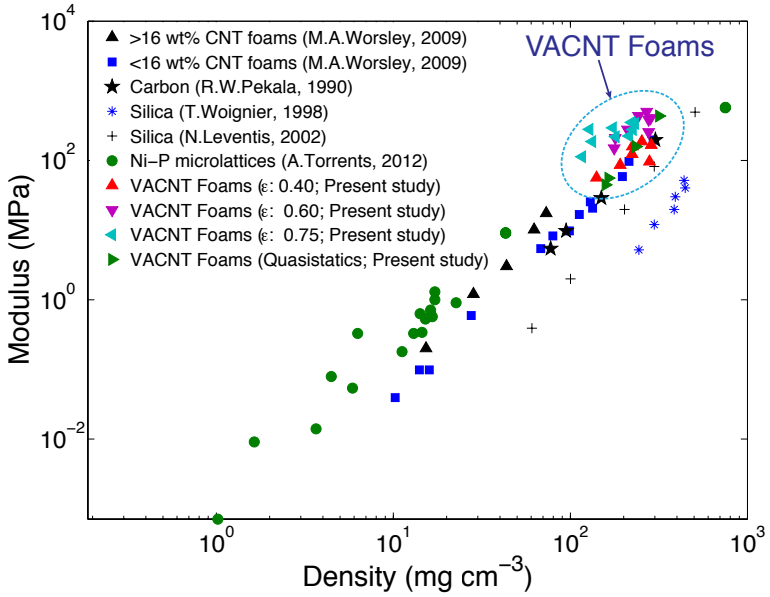

Figure 3.8. Dynamic and quasistatic unloading moduli of VACNT foams as a function of the average bulk density, in comparison with the moduli of similar foam-like materials found in literature [59,148–151].

The *in-situ* visualization using high-speed microscopic imaging provided insights into the fundamental mechanisms of deformations. When the striker impacted the sample, due to the density gradient along the thickness of the VACNT foams, buckling instabilities nucleated in the low-density region of the samples and propagated sequentially towards the high-density region. The initial buckle formation always occurred at the low-density region independently of the impacted side of the sample, implying the strong influence of the intrinsic density gradient. The characteristic intrinsic density gradient measured by synchrotron x-ray scattering and mass attenuation in our samples is shown in the inset of Figure 3.9 (a) (see also Figures 3.2 (a) & (b)). Due to the nonlinear density gradient observed for VACNT foams, when impacted, we observed an increase in buckle wavelength along the height (Supplementary Video 3.1). The samples recovered the deformation upon unloading. A few snapshots of the dynamic deformation are provided in Figure 3.9 (a), along with the corresponding dynamic stress-strain diagram for an

impact velocity of 1.75 m s^{-1}. From Supplementary Video 3.1 it can be seen that the VACNT foams exhibit high resilience to impact with 100% instantaneous recovery. On average, the samples with different densities recovered 83±10% of their dynamic deformation. The characterization of the samples using scanning electron microscopy (SEM) after high velocity impacts (~ 6 m s^{-1}), showed traces of permanent collective buckling (Figure 3.9 (b)). Transmission electron microscopic (TEM) imaging of these specimens revealed individual MWCNTs with wrinkled outer walls (Figure 3.9 (c)). Similar permanent defects of wrinkled outer walls on the compression side of the tube were also reported in earlier dynamic tests of CNT foams [69] and highly bent individual MWCNTs [152].

The *in-situ* visualization using high-speed microscopic imaging provided insights into the fundamental mechanisms of deformations. When the striker impacted the sample, due to the density gradient along the thickness of the VACNT foams, buckling instabilities nucleated in the low-density region of the samples and propagated sequentially towards the high-density region. The initial buckle formation always occurred at the low-density region independently of the impacted side of the sample, implying the strong influence of the intrinsic density gradient. The characteristic intrinsic density gradient measured by synchrotron x-ray scattering and mass attenuation in our samples is shown in the inset of Figure 3.9 (a) (see also Figures 3.2 (a) & (b)). Due to the nonlinear density gradient observed for VACNT foams, when impacted, we observed an increase in buckle wavelength along the height (Supplementary Video 3.1). The samples recovered the deformation upon unloading. A few snapshots of the dynamic deformation are provided in Figure 3.9 (a), along with the corresponding dynamic stress-strain diagram for an impact velocity of 1.75 m s^{-1}. From Supplementary Video 3.1 it can be seen that the VACNT foams exhibit high resilience to impact with 100% instantaneous recovery. On average, the samples with different densities recovered 83±10% of the dynamic deformation. The characterization of the samples using scanning electron microscopy (SEM) after high velocity impacts (~ 6 m s^{-1}), showed traces of permanent collective buckling (Figure 3.9 (b)). Transmission electron microscopic (TEM) imaging of these specimens revealed individual MWCNTs with wrinkled outer walls (Figure 3.9 (c)).

Similar permanent defects of wrinkled outer walls on the compression side of the tube were also reported in earlier dynamic tests of CNT foams [69] and highly bent individual MWCNTs [152].

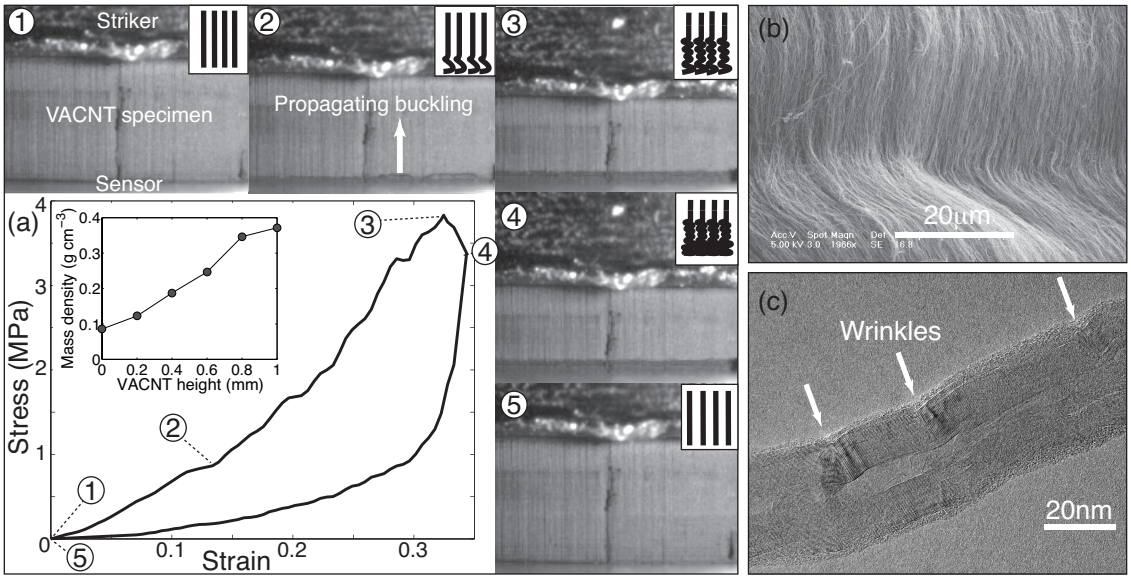

Figure 3.9. (a) Deformation micrographs obtained from high-speed microscopic imaging, for a VACNT foam impacted at 1.75 ms^{-1} (Supplementary Video 3.1); inset shows the intrinsic density variation along the height of a VACNT foam with mean density 0.23 gcm^{-3}. **(b)** SEM image of the collective permanent buckles in a VACNT foam impacted at ~5 ms^{-1} (the scale bar is 20 μm). **(c)** TEM image of an individual multiwalled carbon nanotube exhibiting wrinkles on walls caused by buckling (the scale bar is 20 nm).

The reported rate-independent dynamic loading behavior transitions into shock formation at a critical impact velocity, characteristic of specific bulk densities (Figure 3.10 (a-d)). We have observed this behavior in VACNT foams with a 0.13±0.02 g cm^{-3} average bulk density, at impact velocities of ~ 5 m s^{-1}, and for denser VACNT foams (~0.2 g cm^{-3}), at ~6.5 m s^{-1}. These critical velocities are surprisingly low (more than 10 times lower) compared to the critical shock formation velocities observed in metallic open-cell foams with comparable bulk densities and elastic moduli [153,154] (Aluminum open-cell foams compared here have average bulk density ~0.22 g cm^{-3}; average longitudinal modulus

~593 MPa and transverse modulus ~338 MPa). When the samples were impacted at velocities higher than these critical velocities, we observed a distinct crush front propagating from the low-density region (Supplementary Video 3.2). During the loading phase, the stress increased almost linearly with strain at moderate stress levels. Beyond the densification strain (~0.8), the stress increased rapidly to very high values. During the unloading phase, the stress dropped rapidly and the strain presented a significant recovery (86±8%). A characteristic stress-strain response and the corresponding loading stress-time history for a shocked specimen (with density 0.12 g cm^{-3}, impacted at 5.02 m s^{-1}) are shown in Figure 3.10 (c). A few snapshots from the high-speed image sequence identifying the propagation of the crush front are shown in Figure 3.10 (b). In this case, the stress-strain response of the samples changes dramatically, presenting a much narrower hysteresis, a sharper transition to the densification regime and no characteristic saw-tooth pattern identifying the buckle's formation in quasistatic compression. The crush front in Supplementary Video 3.2 proceeds continuously compressing the samples without allowing time for the sequential buckle formation, seen in the low velocity Supplementary Video 3.1.

The parameters used to calculate the crush front speed and the shock front speed are shown in the schematic diagram in Figure 3.10 (a) [153]. The evolution of the striker velocity (V_m), the crush front velocity (V_c) and the shock velocity (V_s) during the shock compression is shown in Figure 3.10 (d). The time t=166 μs corresponds to the instance the shock reaches the force sensor-VACNT foam interface. During this time, the striker decelerates from 5.02 m s^{-1} to 4.13 m s^{-1}, beyond which it rapidly decelerates to zero as the material is compressed beyond its densification strain. The shock velocity reduces from ~9 m s^{-1} to ~5 m s^{-1} and remains nearly steady until time t=166 μs. The crush front propagates initially at the impact velocity of the striker, and then rapidly reduces to ~0.5 ms^{-1} and remains steady as more material piles up behind the shock. All velocities were calculated by processing the high-speed image sequence using commercial image correlation software (*Image systems, TEMA*). We attribute the presence of oscillations on the shock and the crush front velocities to the discrete time steps of the high-speed image sequence.

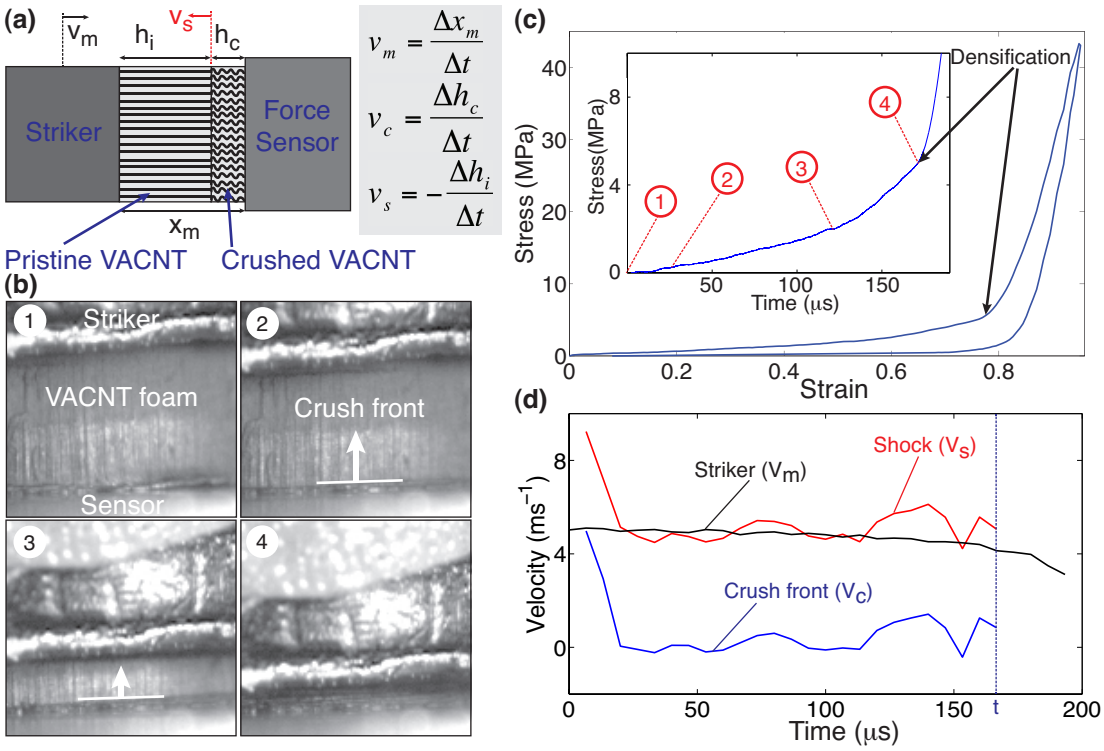

Figure 3.10. (a) Schematic illustration of shock formation in VACNT foams identifying the shock parameters. **(b)** Snapshots from the high-speed camera imaging sequence showing the formation and propagation of the shock wave. **(c)** Stress-strain diagram showing the loading-unloading response during impact. Inset shows the loading phase up to densification; circles 1-4 indicate instances corresponding to the high-speed camera images. **(d)** Evolution of the shock, crush-front and striker velocities during the loading phase. Time *t* indicates the instance when the shock wave reaches the specimen-striker interface, beyond which the crushed VACNT foam is compressed through densification.

The experimental evidence of shock formation in VACNT foams provides critical insights into the influence of graded, fibrous microstructure on the formation and propagation of shock waves. For example, the presence of a density gradient in VACNT foams confines the shock formation in the low-density region of the sample and the shock front progresses towards increasing density. This is reflected also in the stress-time history profile: homogeneous foams present a sharp initial stress increase followed by a plateau-region and densification, whereas VACNT foams show a gradual increase of stress in time, until reaching densification. The presence of fibrous microstructure in the

VACNT foams is responsible for the observed time-scale effects on the micro-scale deformation. In quasi-static or low-velocity impacts, the fibers form progressive buckles undergoing local stiffening followed by local instability. At higher-velocity impacts, the buckle formation does not have sufficient time to progress and it is replaced by progressive crushing.

3.5 Conclusions

VACNT foams present complex rate-effects subjected to impact loadings where loading response is rate-independent and the unloading response is dependent on the strain-rate. When impacted at velocities higher than a critical velocity of impact they support formation and propagation of shock waves. In all cases, VACNT foams exhibit high resilience to impact by recovering more than 80% of the deformation upon unloading. The dynamic energy dissipation characteristics and the mechanical properties are highly controllable, for example by tailoring the foam's microstructure during synthesis varying hydrogen concentration in the carrier gas. We quantified the intrinsic density gradient of the VACNT foams to elucidate the observed fundamental deformation mechanisms. VACNT foams show superior mechanical properties, such as high modulus, compressive strength (peak stress), and energy dissipation characteristics, compared to similar foam-like materials. These properties suggest their use in lightweight materials for tunable vibration damping and energy absorbing applications.